

Vibrational properties of single-wall nanotubes and monolayers of hexagonal BN

D. Sánchez-Portal*

*Centro Mixto CSIC-UPV/EHU and Donostia International Physics Center (DIPC)
Paseo Manuel de Lardizabal 4, 20018 Donostia-San Sebastian, Spain*

E. Hernández[§]

*Institut de Ciència de Materials de Barcelona, ICMA - CSIC,
Campus de Bellaterra, 08193 Bellaterra, Barcelona, Spain*

(Dated: February 1, 2008)

We report a detailed study of the vibrational properties of BN single-walled nanotubes and of the BN monolayer. Our results have been obtained from a well-established Tight-Binding model complemented with an electrostatic model to account for the long-range interactions arising from the polar nature of the material, and which are not included in the Tight-Binding model. Our study provides a wealth of data for the BN monolayer and nanotubes, such as phonon band structure, vibrational density of states, elastic constants, etc. For the nanotubes we obtain the behavior of the optically active modes as a function of the structural parameters, and we compare their frequencies with those derived from a zone-folding treatment applied to the phonon frequencies of the BN monolayer, finding general good agreement between the two.

PACS numbers: 63.22.+m, 62.25.+g, 78.30.Na, 78.20.Bh

I. INTRODUCTION

The discovery of the fullerenes¹ in the mid 1980's, and especially that of carbon nanotubes² in the early 1990's has fueled a frenzy of research activity in the field of carbon nanostructures, doubly motivated by their large potential for practical applications on one hand, and because these systems constitute a new open field for basic research at the nanoscale on the other. Nanotubes can be single-walled or multi-walled, and are quasi-1D structures having large aspect ratios (the quotient of length over diameter). Single-wall carbon nanotubes (SWNTs) can be either semiconducting or metallic, depending on their structural parameters, and can be chiral or achiral. They have large thermal conductivity, and have the highest Young's modulus ever measured^{3,4,5,6}. Nanotubes can be filled with other elements, compounds or even fullerenes in their internal channel, forming structures similar to nanoscale coaxial cables. All these properties confer nanotubes a large potential for technological applications, some of which have already been demonstrated. Nanotubes have been used to fabricate field emission devices⁷, tips for scanning probe microscopy instruments⁸, constituents of nanoelectronic devices⁹, gas sensors¹⁰, composite reinforcement¹¹, lubrication, etc. It is therefore not surprising that these systems have been and continue to be the focus of considerable interest; the large number of review articles¹² and monographs¹³ devoted to the different aspects of fullerenes and nanotubes in recent years provides further proof of this interest.

One of the probes most frequently used to characterize carbon nanotube samples is vibrational spectroscopy, and specifically Raman spectroscopy¹⁴. Raman spectroscopy offers experimentalists a rapid way of estimating the diameter distribution of tubes present in a sample, because the low frequency radial breathing mode (RBM) of

SWNTs has a frequency which is inversely proportional to the square of the nanotube diameter, independently of the nanotube structure, determined by the nanotube indices (n,m). Also, the high frequency G band modes resulting from atomic vibrations in the nanotube shell, can help to distinguish between metallic and semiconducting nanotubes in the sample¹⁵. Jorio and coworkers¹⁶ have recently demonstrated the ability of Raman spectroscopy to provide full structural determinations of isolated carbon SWNT's. The diverse aspects of phonons in carbon SWNT's and the use of Raman spectroscopy as a tool for their characterization have been recently reviewed by Dresselhaus and Eklund¹⁴.

Soon after the discovery of carbon nanotubes it was speculated that other materials could possibly form similar nanostructures, since there are several elements and many compounds which form layered structures bearing some resemblance to graphite. The most obvious candidate was hexagonal BN (h-BN), which was predicted on the basis of theoretical calculations^{17,18} to be capable of forming nanotubes, a prediction which was later corroborated experimentally by the synthesis of such nanotubes¹⁹. Today we know that many other structures can form nanotubes (MoS₂, WS₂²⁰, Bi²¹, ...); nevertheless it is still the case that carbon nanotubes continue to attract a larger interest, but certainly these other structures are interesting in their own right, and may be able to offer different possibilities for technological applications that carbon nanotubes cannot provide. Both multi-walled and single-walled²² BN nanotubes can now be readily synthesized, and these tubes are uniformly insulating, tending to have a zig-zag structure.

As other types of nanotubes become more common, many of the characterization tools and techniques extensively used in the case of carbon nanotubes will undoubtedly also find application in the study of these other

structures. In particular, vibrational spectroscopy, which has proved to be such a useful tool in the case of carbon nanotubes, is likely to prove useful also in these cases. In this context, it is interesting to consider the phonon properties of BN nanotubes from a theoretical point of view; their study will help to develop the characterization potential of spectroscopic techniques when they are applied to BN nanotubes. The aim of this paper is to provide such a theoretical study. We report extensive theoretical calculations of the vibrational properties of a h-BN layer and of a number of BN nanotubes having diameters in the range of 0.4 to 2 nm, including zig-zag, arm-chair and several chiral nanotubes. From our results for the flat sheet we have performed a zone-folding analysis in order to predict the vibrational properties of the tubular structures from those of the flat layer, a technique which has been frequently used in the case of carbon nanotubes. The direct calculation of the vibrational properties of tubular structures allow us to compare the predictions of zone-folding with the actual results, and thus gauge the applicability of the zone-folding approach for BN nanotubes. Other authors have previously considered the vibrational²³ and elastic²⁴ properties of isolated h-BN monolayers and of bulk h-BN^{25,26}. Some aspects of the elasticity of BN nanotubes have also been studied in references 27 and 24. However, the study of the vibrational properties in the case of BN nanotubes has not, to our knowledge, been addressed to date.

The structure of the paper is as follows. In sec. II we describe the model and calculation procedure used in our study; later in sec. III we discuss our findings, starting with a thorough description of the vibrational properties of an isolated h-BN monolayer, followed by the results obtained for the nanotubes, establishing a comparison between the results obtained from the zone-folding analysis and those obtained from direct calculation. Our summary and conclusions are discussed in sec. IV.

II. MODEL AND COMPUTATIONAL PROCEDURE

All calculations have been performed using the non-orthogonal Tight-Binding (TB)²⁸ parametrization of Widani *et al.*²⁹. This is a parametrization following the scheme proposed by Porezag and coworkers³⁰. This model employs a basis set consisting of one S and three P functions per atom, to represent valence states, and the resulting Hamiltonian and overlap matrix elements extend up to a range of approximately 5 Å. The core-core repulsion is modeled by means of a simple pair-repulsive potential. The original work of Porezag *et al.*³⁰ described a non self-consistent TB model; although an extension of the methodology has been proposed which incorporates some degree of self-consistency³¹, here we only have used the model of Widani²⁹ in its non self-consistent form. It is worth commenting that in spite of its simplicity this model has proved to be quite successful^{27,29}.

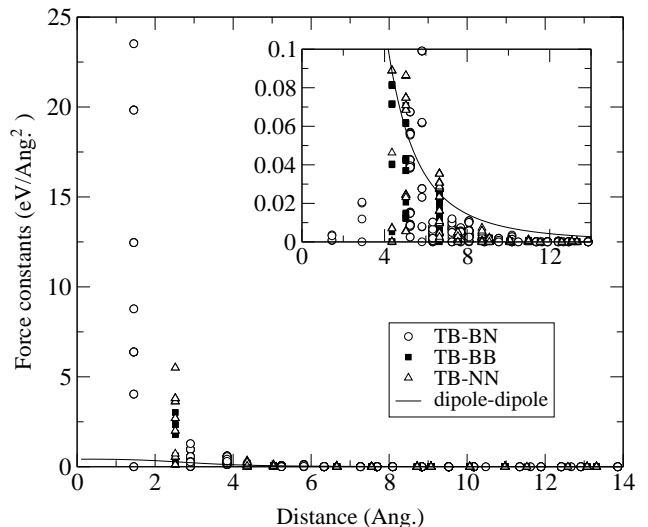


FIG. 1: Force constants derived from the TB model (symbols) and the typical behavior of the electrostatic interactions (approximated in the plot by $f(r) Z_{||}^2 / (\epsilon r^3)$) (solid line), as a function of distance. The inset shows more clearly the behavior for large distances.

The equilibrium structures of the tubes were obtained by careful minimization of the total energy with respect to both the atomic coordinates and the lattice constant along the tube axis. For the phonon calculations, we then computed the force-constant matrix in real space using a finite-difference approach³². We used atomic displacements of 0.02 Å, and the force constants were taken as the average of the results obtained with positive and negative displacements, in order to eliminate anharmonic effects. Since all nitrogen and boron atoms are equivalent by symmetry in the tubes, we only calculated the force constants for one nitrogen and one boron atom in the supercell and generated the rest of the matrix using the symmetry operations.

The force-constants have to be calculated between a given atom and all the other atoms in the system. However, since the interactions in our TB model decrease rapidly with distance, only the elements with atoms sufficiently close have to be computed. To do so, we set up a supercell large enough that a sufficient number of neighbors is included. It must be kept in mind that, in the supercell geometry, a given atomic displacement in the central cell is always accompanied by the same displacement of all image atoms. We need, therefore, to use a supercell such that the effect of the image displacements is negligible. For this purpose we have used supercells containing six unitcells in the case of (n,n) and (n,0) tubes, and two and one unitcells, respectively, in the case of the (10,5) and (10,7) tubes. The supercells contain hence a

minimum of 144 atoms for the (6,0) and (6,6) tubes, and a maximum of 384 atoms in the case of the (16,0) tube.

The above described TB model does not by itself incorporate any long-range electrostatic interactions. Such interactions are important when considering the vibrational properties of polar materials, because they will make a long-range contribution to the force constants. Therefore we have opted for correcting this shortcoming in the TB model in a physically sound but otherwise empirical way. The key observation in order to introduce the effects of the electrostatic interactions is that, when an atom i suffers a displacement $\mathbf{u}(i)$ from its equilibrium position, a net electric dipole of magnitude $\mathbf{p}^i = \sum_{\mu} Z_{\nu\mu}^i u_{\mu}^i$ appears associated with this atomic movement³³. Here $Z_{\nu\mu}^i$ is the Born effective charge tensor³³ of the atom i . As a consequence, if two atoms i and j are simultaneously displaced from their positions, besides the interaction energy given by our TB model, it is necessary to include the long-range interaction between the two electric dipoles generated. This gives rise to a new term in the force-constants matrix of the form³³

$$C_{\nu\mu}^{LR}(\mathbf{r}_{ij}) = f(r_{ij}) \sum_{\nu'\mu'} \frac{Z_{\nu\nu'}^i Z_{\mu\mu'}^j}{\epsilon} \left(\frac{\delta_{\nu'\mu'}}{r_{ij}^3} - 3 \frac{r_{ij\nu'} r_{ij\mu'}}{r_{ij}^5} \right), \quad (1)$$

where the superindex LR in $C_{\nu\mu}^{LR}(\mathbf{r}_{ij})$ indicates that this is the long-range contribution to the force constants; $f(r_{ij})$ is a switching function (see below), ϵ is the dielectric constant, \mathbf{r}_{ij} is the vector going from atom i to atom j , and r_{ij} is the distance between these two atoms. The switching function is designed to come into play at distances sufficiently large so as to not affect the TB model; it takes the form

$$f(r) = 1 - e^{-(r/r_c)^3}. \quad (2)$$

Following the usual approach³³, it is also necessary to modify the on-site elements of the force matrix in order to satisfy the acoustic sum rule. Therefore, we take

$$C_{\nu\mu}^{LR}(\mathbf{0}_{ii}) = - \sum_{j \neq i} C_{\nu\mu}^{LR}(\mathbf{r}_{ij}). \quad (3)$$

The Born effective charge tensor has been taken from recent *ab initio* density functional calculations²⁶: $Z_{\perp}^B = -Z_{\perp}^N = 0.82$ for out-of-plane, and $Z_{\parallel}^B = -Z_{\parallel}^N = 2.71$ for in-plane displacements³⁴. We have taken $\epsilon = 4$ and $r_c = 2.6$ Å, the distance of separation between second nearest neighbors in the h-BN layer. We have not attempted to fit these values in order to improve agreement of our results with experimental measurements. Rather, our approach has been to take reasonable values for them in order to estimate the effect of the polar interactions on the vibrational properties of the BN monolayer and in the nanotubes. Our chosen value for ϵ is close to the experimental one for h-BN (4-5 depending on the direction^{26,35}), and the value of r_c used in Eq. (2) is motivated by the fact that force constants arising from the

TB model alone decay very rapidly with distance, and they are already very small at this value of r_c , as can be seen in Fig. 1. By choosing r_c equal to the second nearest neighbor distance we ensure a smooth switching between the short-range TB model and the long-range electrostatic one, with minimum interference between them.

Once we have the force-constant matrix in real space, we can calculate the dynamical matrix in reciprocal space, and diagonalize it to obtain the phonon modes and frequencies. In the case of bulk polar systems the computation of the dynamical matrix in reciprocal space has to be made with some care. The reason is that, due to the long-range nature of the dipole-dipole interaction in Eq.(2), a different limit for the dynamical matrix is obtained, as the phonon wavevector \mathbf{k} approaches $\mathbf{\Gamma}$, in the cases of longitudinal and transversal vibrations. In our case however, due to the reduced dimensionality of the systems considered (a monolayer and single-walled tubes), the Fourier transform of the dynamical matrix can be performed without further complications by simply adding up the elements of the real-space matrix with the appropriate phase factors. Given its simple analytical form, we can include a large number of neighbors (we typically take all neighbors within a radius of ~ 200 Å) in the summation involving the dipole-dipole interactions and guarantee a good convergence. The same limit is found for both polarizations when $\mathbf{k} \rightarrow \mathbf{\Gamma}$, and there are no splittings between in-plane longitudinal and transversal optical modes at $\mathbf{\Gamma}$ (see Appendix).

III. RESULTS AND DISCUSSION

One of the aims of this work is to judge the validity of the zone-folding approach for obtaining phonon information of tubular structures from the phonon band structure of the flat sheet, a procedure which has been frequently used in the case of carbon nanotubes¹⁴. To this end we have performed a phonon analysis of the flat sheet, and of several nanotubes (arm-chair, zig-zag and chiral) so as to compare the zone-folding results with those obtained directly from the tubular structures. In the following we will first present the results obtained for the flat sheet, followed by those for a selected set of nanotubes. The comparison between these latter results and the zone-folding predictions will be then presented.

A. Flat sheet

Using the TB model discussed in section II, with and without the dipolar interactions, with a supercell containing 192 atoms we have obtained the phonon dispersion curves and vibrational density of states for a flat sheet of h-BN, plotted in Fig. 2. In order to check the convergence of the results with respect to the supercell size, we performed a test with a supercell containing 320 atoms; the results obtained with the smaller cell are in-

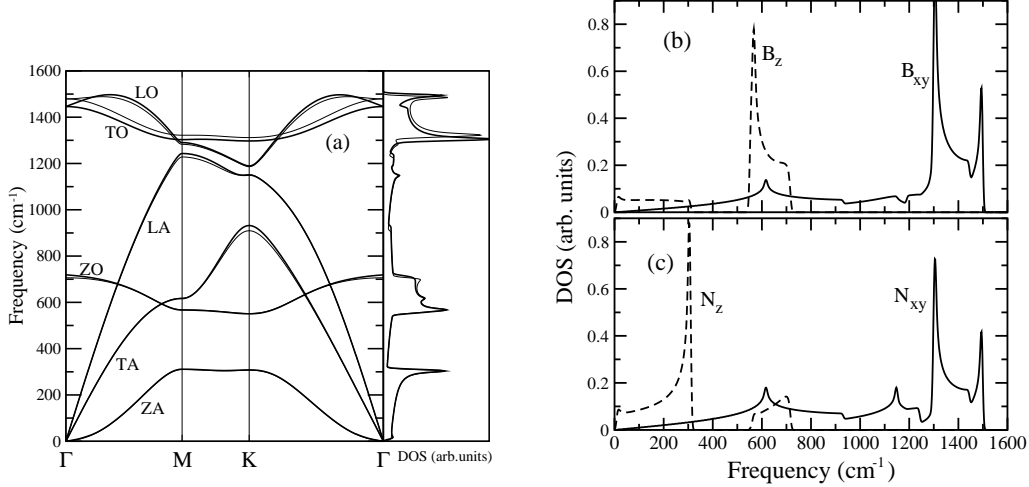


FIG. 2: (a) Phonon band structure of the BN hexagonal monolayer (right) and the corresponding density of vibrational states (left); thick lines correspond to band structure and density of states calculated with electrostatic interactions included, while thin lines give results obtained only with the TB model. (b) Projected density of states on the B atoms; continuous line represents the density of states projected onto the plane of the monolayer, while the discontinuous line gives the density of states projected perpendicular to the plane of the monolayer. (c) As in (b) for the N atoms.

distinguishable from those of the larger cell, and hence all subsequent analysis was performed with the 192 atom cell results. We also performed a more detailed analysis of the convergence of the phonon bands with respect to the lower threshold of the elements of the real-space force-constant matrix included in the construction of the dynamical matrix. We focus first on the convergence with respect to the TB force constants. We found that including all the couplings coming from the TB hamiltonian with absolute value larger than $1.2 \times 10^{-2} \text{ eV/\AA}^2$ was necessary to adequately converge all bands. This threshold corresponds to a spatial cutoff of 6.7 \AA , which includes all atoms within the tenth nearest-neighbor shell. This large cutoff is required to correctly reproduce the quadratic behavior of the lowest acoustic band [labeled ZA in Fig.2] in the limit $\mathbf{k} \rightarrow \Gamma$, with a zero sound velocity (slope of the band) as \mathbf{k} approaches Γ . This quadratic behavior of the ZA band is a consequence of the fact that, at least to the lowest order in its amplitude, the strain energy created by this vibration is solely associated with the curvature that this out-of-plane bending mode induces in the layer. Optical bands typically converge much faster (*ca.* including interactions with neighbors within the third or fourth nearest-neighbor shell). It is worth mentioning in this respect that in the earlier theoretical

work of Miyamoto *et al.*²³ a supercell which only permitted the inclusion of second nearest neighbor interactions was used due to computational limitations (Miyamoto and coworkers used first-principles methods, which are significantly more costly, to evaluate the force-constant matrix). Although inclusion of up to second nearest neighbor interactions is sufficient to adequately converge most bands, it fails to reproduce the over-bending (see below) of the longitudinal-optical (LO) band, for which the maximum occurs not at Γ but approximately half way along the symmetry lines $\Gamma - \text{M}$ and $\Gamma - \text{K}$, and is insufficient to reproduce the quadratic behavior of lowest acoustic band around Γ .

Let us now comment briefly on the convergence with respect to the long-range electrostatic interactions. As already commented in the previous section, due to its simple analytical form we have used a large cut-off of 200 \AA for the dipole-dipole interactions. However, we have checked that already with a cut-off of $\sim 25 \text{ \AA}$ the results are well converged. Further reducing the interaction range starts to have an appreciable effect. Not only the position of the optical branches at and close to Γ start to shift from their converged values, but the finite slope at Γ that the LO mode must exhibit as a consequence of the long-range nature of the interactions also disappears

| | |
|--------------------------|---------------|
| $C_{xxxx} \equiv C_{11}$ | 0.343 (0.322) |
| $C_{xxyy} \equiv C_{12}$ | 0.119 |
| $C_{xyxy} \equiv C_{66}$ | 0.107 (0.123) |
| Y | 0.302 |
| σ | 0.347 |

TABLE I: Elastic constants and Young modulus Y , in units of TPa nm, and Poisson ratio σ of the flat BN hexagonal sheet, as calculated directly from the force-constant matrix given by our model. The results obtained from the sound velocities of the TA and LA bands (see Eq.(5)) are shown in brackets.

(see Appendix).

As can be appreciated in Fig. 2, due to the two-dimensional character of the system, there is a separation between in-plane and out-of-plane modes, the latter being the lower frequency ones, with a maximum at Γ of 719 cm^{-1} with dipolar interactions included (706 cm^{-1} if these are not included). This frequency separation is to be expected, since in-plane modes excite both bond-stretchings (hard) and bond-bendings (soft), while out-of-plane modes result mostly in bond-bending motion and very little bond-stretching. The highest frequency bands, the LO and the transversal-optical (TO), have a frequency at Γ of 1446 cm^{-1} when the dipolar interactions are included (1479 cm^{-1} without). The maximum of the LO band occurs not at Γ , but at an intermediate point away from the Brillouin zone edges, as pointed out above. This is known as over-bending, and the presence of over-bending in the flat sheet phonon band structure can have interesting consequences for the phonon band structure of the nanotubes, as it may lead to the appearance of new modes at Γ having higher frequencies in the tubular structures than in the flat sheet³⁶. Note that including the dipolar interactions increases the over-bending, which is much smaller when the electrostatics are not appropriately accounted for. Another noteworthy characteristic of the phonon band structure displayed in Fig. 2(a) is the splitting of approximately 250 cm^{-1} existing between the ZO and ZA bands along $\mathbf{M-K}$. In a homopolar hexagonal sheet such as graphene these two bands cross at \mathbf{K} ³⁷.

From the slopes of the transversal-acoustic (TA) and longitudinal-acoustic (LA) bands in the limit $\mathbf{k} \rightarrow \Gamma$ we deduce a sound velocity of 13 Km/s and 21 Km/s , respectively. As already pointed out above, the ZA band exhibits a k^2 behavior in this limit, as expected, and therefore the sound velocity associated to this band is zero. Fitting the frequencies below 250 cm^{-1} to the expression $\omega = 2\pi\nu = \delta k^2 + \gamma k^3$, we can estimate a value of $\delta \approx 1820 \pm 60 \text{ cm}^{-1} \text{ \AA}^2 = 5.5 \pm 0.2 \times 10^{-7} \text{ m}^2 \text{ s}^{-1}$. This parameter is interesting because it allows to estimate the energy necessary to roll up the BN sheet in order to form the nanotubes. Simple arguments show that the strain energy per atom can be approximated by $E_{st} = C/r^2$ with $C = \delta^2(m_N + m_B)/4$, being m_N and m_B the masses of

the nitrogen and boron atoms, respectively, and r the tube radius. The value obtained for C in this way is 1.91 eV \AA^2 , which is in reasonable agreement with the magnitude obtained from total energy calculations performed using both, a tight-binding hamiltonian similar to the one utilized here²⁷, and first-principles density functional calculations^{18,24}. A similar estimation in the case of graphene³⁷ ($\delta \approx 6 \times 10^{-7} \text{ m}^2 \text{ s}^{-1}$) leads to a value $C \approx 2.3 \text{ eV \AA}^2$. Therefore, already looking at the phonon band structures it is possible to find an indication that the strain energy is smaller in the case of BN tubes than for carbon nanotubes, a result which is confirmed by more sophisticated calculations.^{18,24,27,38}

Using the calculated force-constants matrix we can directly obtain the elastic constants³⁹ of the flat sheet, which are given in Table I. In bulk three-dimensional systems it is customary to quote elastic constants in units of pressure, due to the inverse equilibrium cell volume factor that appears in the definition of the elastic constants^{39,40}. However, in two-dimensional systems the definition of the cell volume is arbitrary, and it is therefore more appropriate to use cell area in the definition of the elastic constants²⁷; hence, we provide our results in units of pressure times length. Comparing with previous calculations in the literature, our result for C_{xxxx} is in reasonable agreement with the value of 0.271 TPa nm obtained for the in-plane stiffness⁴¹ by Kudin and coworkers using density-functional theory and Gaussian type orbitals²⁴. Our result is also in quite good agreement with the value of 0.309 TPa nm that can be deduced from the plane-wave density-functional calculation of the elastic constants of bulk h-BN reported by Ohba *et al.* in Ref. 26 (we use here the calculated interlayer distance of 3.25 \AA to translate the data from the bulk to the monolayer geometry). However, the comparison is poorer for the C_{xyxy} elastic constant, for which the data of Ohba and coworkers translate into 0.055 TPa nm for the monolayer (roughly half our value). The origin of this large discrepancy is unclear, although it might be related to the interactions with neighboring layers, which are not present in our case.

For a hexagonal two-dimensional crystal only two elastic constants are required⁴², and due to the underlying crystal symmetry we obtain the following rule:

$$C_{xxxx} = C_{xxyy} + 2C_{xyxy}. \quad (4)$$

This provides an internal consistency check for our results, which, as can be seen from the results in Table I, is satisfactorily obeyed [the numerical value obtained for C_{xxxx} using C_{xxyy} and C_{xyxy} in Eq. (4) is within 3 % of its calculated value, given in Table I]. A second consistency check is provided by the comparison of these values of the elastic constants with those obtained from the sound velocities reported above using the identities

$$v_{LA}^{2D} = \sqrt{\frac{C_{xxxx}}{\rho}}, \quad v_{TA}^{2D} = \sqrt{\frac{C_{xyxy}}{\rho}}, \quad (5)$$

where ρ is the surface mass density of the sheet. These data are also given in Table I. As can be seen there, the values obtained in these different fashions are in rather good agreement. From the elastic constants we can also calculate⁴² the Poisson ratio,

$$\sigma = \frac{C_{xyxy}}{C_{xxxx}}, \quad (6)$$

and Young's modulus,

$$Y = \frac{C_{xxxx}^2 - C_{xyxy}^2}{C_{xxxx}}. \quad (7)$$

The values obtained for σ and Y are also given in Table I. These values can be compared with those obtained previously for BN nanotubes using the same TB model²⁷; the value of σ obtained here is a little bit larger than that obtained for the nanotubes (0.263), but the agreement with the tube Young's modulus (0.298-0.310 TPa nm depending on the tube diameter) is nearly perfect. We also point out that the inclusion of the dipolar interactions does not affect the values of the sound velocities or elastic constants, as expected from the fact that they only influence the high frequency optical phonon bands, but not the acoustic ones, as can be seen in Fig. 2.

At the zone edge the ZA band corresponds mostly to N atom out-of-plane displacements, while the ZO mode corresponds to B displacements. This is most clearly seen in Fig. 2(b) and (c), which shows the partial vibrational density of states (DOS) separated into its in-plane and out-of-plane atomic contributions.

The frequency of the Raman and infrared-active (IR) modes in bulk h-BN has been investigated by several authors^{35,43,44,45} obtaining similar results. The values reported for the high energy Raman-active E_{2g} mode are 1366^{43,44}, 1367⁴⁵, and 1370³⁵ cm⁻¹. For the IR modes the values given in the literature are: 1367³⁵ and 1383 \pm 5⁴⁵ cm⁻¹ for the $E_{1u}(\text{TO})$ mode, 1610³⁵ cm⁻¹ for the $E_{1u}(\text{LO})$ mode, and 770 \pm 3⁴⁵ and 783³⁵ cm⁻¹ for the $A_{2u}(\text{TO})$ mode. At this point it is important to note that, since our calculations refer to a free-standing (isolated) flat sheet of h-BN rather than to the bulk material, the comparison with these experimental observations has to be made with some care. In analogy to the case of graphite, and assuming relatively weak inter-layer interactions, the frequencies of a single BN sheet should be closely related to those of the bulk. However, there is an important exception related to the role of the long-range electrostatic interactions. In a strictly two-dimensional (2D) system like the one treated here (*i.e.* a sheet of monatomic thickness), the electrostatic interactions do not result in a macroscopic term at Γ for in-plane modes, and hence we do not obtain any LO-TO splitting in that limit (see Appendix). This striking difference is quite notorious, for example, comparing our phonon band structure in Fig. 2(a) with the calculations for bulk h-BN displayed in Fig. 3 of Ref. 25. The absence of LO-TO splitting for the systems of reduced dimensionality

considered here turns out to be quite important when considering the applicability of the zone-folding approach to the vibrational properties of BN nanotubes, a point to which we will return below.

Our results for the planar BN sheet have, therefore, to be compared with the TO frequencies of the bulk. We obtain for the highest modes at Γ a frequency of 1446 cm⁻¹, to be compared against the empirical values of the E_{2g} and $E_{1u}(\text{TO})$ modes, and 719 cm⁻¹ for the ZO mode, to compare with the measurements for the $A_{2u}(\text{TO})$. The discrepancies are therefore smaller than 10 %, which we regard as acceptable, given the simplicity of the TB model employed in this work. It is noteworthy that the effect of the inclusion of the long-range electrostatic interactions improves the comparison with experiment, correcting the under-estimation of the ZO(Γ) frequency and the over-estimation of the TO(Γ) and LO(Γ) value, as well as giving a more realistic over-bending of these modes along $\Gamma - \text{M}$ and $\text{K} - \Gamma$. We should emphasize here that no empirical information on vibrational or structural properties has been used in the construction and parametrization of the model²⁹. As pointed out above, it is also important to take into account that at least some of the discrepancy may not be attributed to the model, but to the geometry used in the supercell calculation. The presence of near-by sheets in the experiment is likely to soften somewhat the in-plane LO and TO modes, while hardening the ZO mode, which could account for some of the discrepancy between our results and the experimental ones. Discrepancies of similar size also occur between the first-principles values of Miyamoto *et al.*²³ and the experimental values. The overall topology of our phonon band structure is in good agreement with the results of Miyamoto *et al.*, although we cannot make a direct comparison due to the unusual shape of the h-BN supercell used in that work. Kern *et al.*²⁵ have also performed first-principles density functional calculations of the phonon properties of both cubic and h-BN. Our phonon band structure is in reasonable agreement with that obtained by them, bearing in mind the different methodologies and geometries used in their work and ours.

Rokuta *et al.*⁴⁶ have obtained the phonon spectra of a BN monolayer deposited over a series of metal surfaces (Ni, Pd and Pt) using high resolution electron energy loss spectroscopy. Again, there is overall good agreement between the results reported by Rokuta and coworkers, and our own. Interestingly, they find no splitting at Γ between the LO and TO modes when the BN monolayer is placed over a Ni(111) surface, but some splitting is seen when the other metals are used. This result was considered as quite surprising by these authors, especially taking into account that Ni(111) was the sole substrate on which BN formed well ordered commensurate monolayers, and it was suggested that this is because Ni can effectively screen the polarization field of the LO mode, while Pd and Pt cannot. However, we maintain that the polarization field only arises in 3D systems; in the 2D

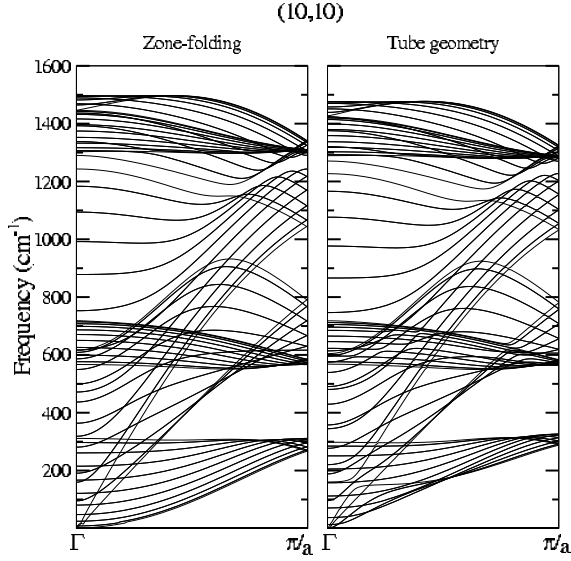


FIG. 3: Comparison of the the phonon dispersion curves of the (10,10) tube (40 atoms in the unit cell and a diameter of 13.9 Å) calculated directly from the tube structure, and those obtained using the zone-folding approach from the results for the flat sheet shown in Fig.(2a).

case the electrostatic interactions do not give rise to a macroscopic field for in-plane modes, *i.e.* the field has zero component at Γ , and hence there is no splitting of the TO and LO bands in that limit. However, the electrostatic interactions do give rise to non-zero components of the field in regions of the Brillouin zone away from Γ , and these result in a higher over-bending when the electrostatic interactions are included. Another consequence of the inclusion of the electrostatic interactions is the fact that the LO mode approaches Γ with a finite slope, which does not occur when the electrostatics are not included [see Fig. 2(a)].

Prompted by this experimental study, we have considered the effect of the presence of an ideal metal surface in the proximity of the BN layer on the phonon properties of the latter. The metal surface is simply considered as a medium which generates dipolar images of the BN monolayer. The net result is to effectively shorten the range of the electrostatic interactions: the finite slope of the LO mode at Γ is lost, and although quadrupolar interactions persist in the BN-metal surface system, the dipolar interactions are screened out.

Interestingly, Rokuta *et al.*⁴⁶ report a degeneracy of the ZO and ZA modes at \mathbf{K} . This is unexpected, because such modes should display a splitting related to the different masses of B and N. The fact that no splitting is observed in the experiments is probably a result of a deviation from planarity in the BN monolayer due to the presence of the metal surface. Another important point

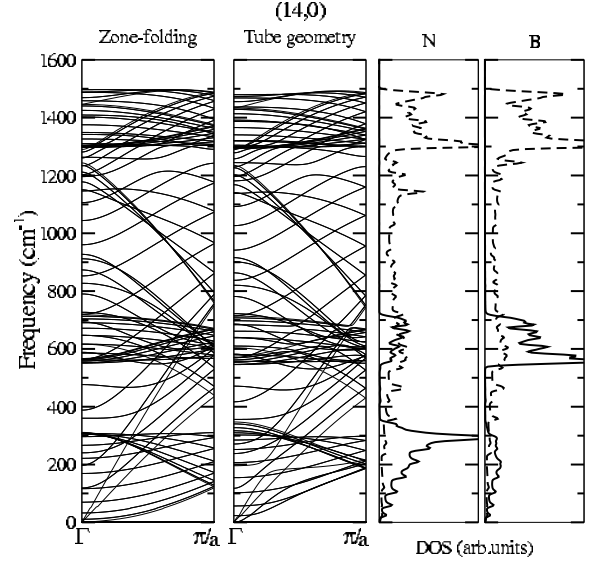


FIG. 4: Same as Fig. 3 for the (14,0) tube (56 atoms in the unit cell and a diameter of 11.3 Å). The vibrational density of states decomposed in the different directions of the atomic displacements is also shown. Solid lines for out-of-plane displacements and dashed lines for in-plane displacements.

might be the quite different positions occupied by B and N atoms on the surface. In fact, Rokuta and coworkers reported a buckling of the BN monolayers on Ni(111), where B atoms, which occupy fcc sites, lie 0.2 Å below the N atoms, which sit directly on top of the Ni atoms in the surface.

B. Nanotubes

Let us now move on to discuss the results obtained for BN nanotubes. We have considered a series of (n,n) (arm-chair), (n,0) (zig-zag) and (n,m) ($n \neq m \neq 0$, chiral) nanotubes. For (n,0) nanotubes we have included all tubes with n from 6 to 16, *i.e.* diameters from 5 to 14 Å, approximately; while for (n,n) tubes we considered specifically the (6,6), (10,10) and (15,15) tubes, with diameters between 8 and 21 Å. Only two chiral nanotubes were considered, since these structures usually have very large unit-cells, namely the (10,5) and (10,7) tubes, with diameters of 10.6 and 11.9 Å, respectively.

In Fig. 3, for the (10,10) tube, and Fig. 4, for the (14,0), we compare the phonon dispersion curves calculated directly from the tube structure, and those obtained for the same tubes employing the zone-folding approach from the phonon bands of the flat sheet discussed above. Firstly, let us remark that the zone-folding method cannot reproduce certain low energy modes; in particular, it cannot give rise to a breathing mode, which in the flat sheet cor-

responds to a zero energy translation perpendicular to the plane. However, the high frequency modes are expected (and indeed are) to be reasonably well described. In spite of the limitation regarding low frequency modes, the zone-folding approach has been extensively used for the interpretation of experimental results of carbon nanotube vibrational modes^{14,36}, partly due to its simplicity, and also to the fact that the phonon modes of graphite can be determined with very high accuracy. One of the aims of the present paper is to study if the zone-folding approximation can also be useful in the case of the BN nanotubes.

Generally speaking, for experimentally relevant tube diameters, the zone-folding method reproduces quite well the overall phonon band structure. Deviations can be larger for the smaller nanotubes, where the effects of curvature are more noticeable. In particular, we shall see below how curvature effects influence the breathing mode. Another difference that can be appreciated between the tube dispersion bands and those determined from zone-folding is a general softening of frequencies for the explicit calculation, where curvature effects are taken into account. The downward shift is especially clear at high frequencies, but is also noticeable at intermediate ones. This shift is not homogeneous, and it has also a non-trivial dependence on the wave vector and on the nature of the mode (radial or tangential).

Also shown in Fig. 4 is the vibrational DOS for the (14,0) tube decomposed in the different directions of the atomic displacements. This curve resembles closely the result obtained for the BN monolayer. There is a clear energy separation between radial and tangential modes (parallel or perpendicular to the tube axis), the radial modes corresponding to frequencies below $\sim 700 \text{ cm}^{-1}$. This corresponds to the already mentioned separation between out-of-plane and in-plane-modes in the case of the planar sheet, as could be expected, since the radial modes are roughly derived from the out-of-plane vibrations of the plane.

There are four acoustic bands for the tubes. They correspond to a longitudinal mode (atomic displacements parallel to the tube axis), two degenerate transversal modes (atomic displacements perpendicular to the tube axis), and a torsion of the tube around its axis (the so-called *twiston* band which, in the limit of $\mathbf{k}=0$, generates a rigid rotation of the tube around its axis). This last mode is characteristic of a one-dimensional system like the nanotubes, and no analog can be found for the bulk or the infinite planar sheet. According to Saito *et al.*⁴⁷, and in contrast to the case of the flat sheet, all four bands would be required to approach Γ linearly. This relates to the fact that none of the acoustic bands of the nanotubes is solely derived from the quadratic out-of-plane acoustic band of the sheet: the transversal acoustic bands can be regarded as a combination of the TA in-plane and ZA out-of-plane modes of the planar sheet. However, it is interesting to point out here that the low energy behavior of the transversal acoustic bands in the nanotubes is

still the subject of some controversy and some authors have recently proposed that these bands should exhibit a quadratic behaviour for small values of \mathbf{k} ^{48,49}. The situation is more clear for the other acoustic bands since it is possible to establish a one-to-one correspondence between the longitudinal and twiston bands of the tubes and the LA and TA bands of the planar sheet, respectively. In fact, the sound velocities of the latter bands are, within the precision of the calculations ($\sim 1 \text{ Km/s}$), independent of the tube radius and chirality, and almost identical (although somewhat smaller) to those of the corresponding planar-sheet bands. Similar results have been obtained for the case of the carbon nanotubes^{47,50}. This insensitivity to the tube structure and radius confirms the predictions of a simple continuum elasticity model of the tubes⁵¹ where the elastic constants are directly taken from the planar sheet, from which one obtains $v_{LA}^{tube} = v_{LA}^{2D}$ and $v_{twiston}^{tube} = v_{TA}^{2D}$. The independence of the mechanical properties on the chirality of the tubes is here a simple consequence of the isotropy of the underlying hexagonal structure of the BN planes. We have used this model to estimate the sound velocity of the transversal band, obtaining $v_{TA}^{tube} = \sqrt{\frac{1}{2}} v_{TA}^{2D} = 9 \text{ Km/s}$. In the TB calculations, however, the transversal bands seem to be more sensitive to the numerical uncertainties than the other acoustic bands, being difficult to extract an accurate slope. In fact, although the transversal bands apparently exhibit a linear dependence with the phonon wavevector (see figures 3 and 4), for very small values of \mathbf{k} , and consequently for very small frequencies, they seem to bend slightly. This would be roughly consistent with the proposed^{48,49} quadratic behavior, although problems of numerical accuracy cannot be ruled out. The clarification of this point will be the subject of future work. Here we have decided to make an estimation of the sound velocity of the transversal modes from the slope of these bands in the region where they still exhibit a clear linear behaviour. In this way we have found values ranging from 7 Km/s, for the narrower tubes, to 8 Km/s, for those with larger diameters. This is again in reasonable agreement with the result that we obtained from continuum elasticity theory.

In Fig. 5 we have plotted the frequencies of the optically active modes for the different tubes considered as a function of the tube radius⁵². The values plotted have been obtained including the long range electrostatic interactions, but the picture does not change significantly if they are not included⁵³. We have classified the modes according to the corresponding symmetry point group⁵⁴, which for zig-zag (n,0) nanotubes is C_{2nv} , for arm-chair (n,n) nanotubes is C_{2nh} , and for chiral (n,m) nanotubes is C_N , where $N=2(n^2+m^2+nm)/d_R$ with d_R being the greatest common divisor of $2n+m$ and $2m+n$ ⁵⁴, *i.e.* $N=70$ for the (10,5) nanotube, and $N=146$ for the (10,7) nanotube. The total number of Raman and IR active modes and their distribution over the frequency spectrum is very similar for both zig-zag and chiral nanotubes. In the (n,0) nanotubes the rotationally invariant

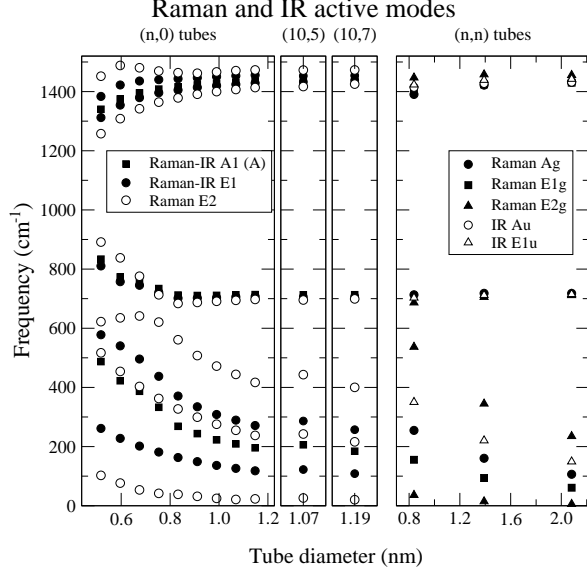


FIG. 5: Active modes for the (n,0), chiral and (n,n) BN nanotubes considered in this work. Symbols have the same meaning for (n,0) and chiral tubes, except that for chiral tubes A1 has to be read as A (see the text). See Ref. 52 for the numerical values of the frequencies.

modes can be classified according to how they transform under reflection through the symmetry plane σ_v , namely A_1 and A_2 modes; only the first are Raman and IR active, the A_2 being inactive. The chiral tubes do not contain a σ_v mirror plane, and therefore all six A modes are active. In total, the (n,0) nanotubes have eight modes with non-zero frequency which are both IR and Raman active (three belong to the A_1 representation, and five to the E_1), and six modes (E_2) which are only Raman active, while for the chiral tubes the count is nine IR and Raman modes (four A and five E_1), plus six (E_2) Raman active modes⁵⁴. In the case of the (n,n) nanotubes, due to the existence of inversion symmetry in the point group the active modes can only be either IR or Raman active, having a total of four IR active (one A_u and three E_{1u}) and nine Raman (three A_g , two E_{1g} and four E_{2g}) active modes. Comparing with carbon nanotubes, the bigger difference appears in the case of the (n,0) nanotubes, where the number of active modes is nearly double for BN nanotubes than for carbon nanotubes⁵⁵.

In Fig. 6(a) we have plotted the frequency of the breathing mode as a function of the tube radius. This mode is of importance in carbon nanotubes because it can be correlated with the tube radius and it is Raman active

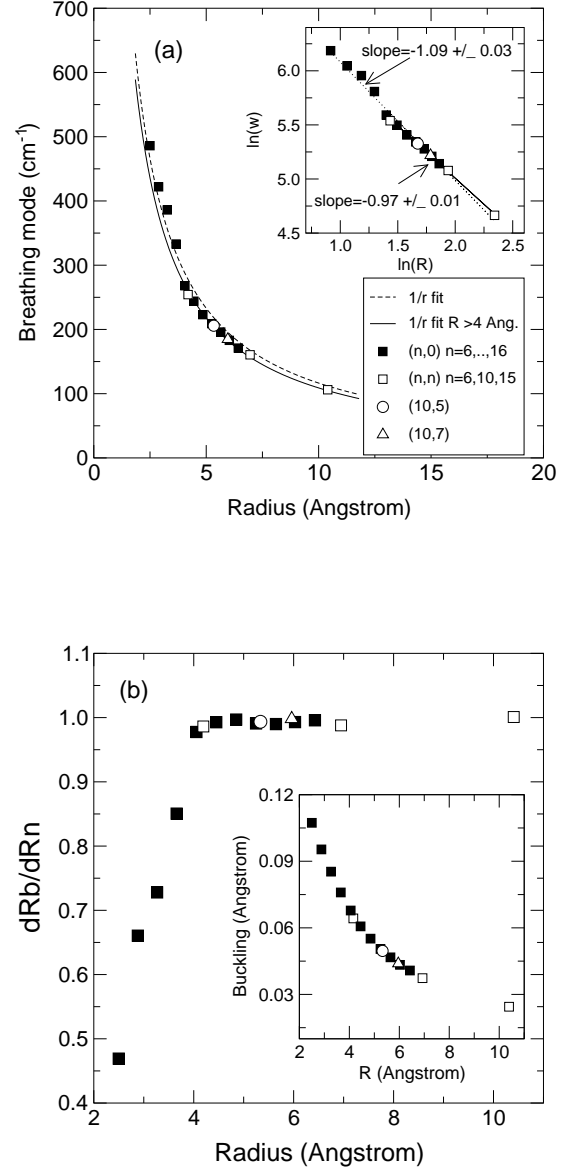


FIG. 6: (a) Frequency of the radial breathing mode of BN nanotubes as a function of tube radius. The inset presents a log-log plot which clearly shows the r^{-1} behavior. Panel(b) shows the relative radial displacement of the B atoms and the N atoms in the radial breathing mode. The evolution of the buckling in the nanotube structure is plotted in the inset as a function of the radius. The meaning of the symbols is identical in all the panels and plots. See Ref. 52 for the numerical values of the frequencies.

for all tube chiralities. The same is true here. Although there are minor deviations at small radii (below 4 Å), the breathing mode frequency follows very closely a dependence on the inverse of the tube radius: $\nu_{BM}(r) = A/r$. This is corroborated in the log-log plot shown in the inset

of Fig. 6(a), which fits very well to a linear behavior with a slope -0.97 ± 0.01 (-1.09 ± 0.03 including the tubes with $r < 4$ Å). Leaving out the tubes with $r < 4$ Å, a fit to this expression gives $A = 1091 \text{ cm}^{-1}\text{Å}$, with a standard deviation smaller than 3 cm^{-1} . This value is quite insensitive to the tube structure, as occurs also with carbon nanotubes^{37,56}. As can be seen in Fig. 6(a), the breathing mode exhibits a hardening for the smaller structures ($r < 4$ Å) respect to what would be expected from the r^{-1} fit to the frequencies of the tubes with the larger diameters. If we include the frequencies of the smaller tubes, the quality of the fit decreases (mean deviation of 16 cm^{-1}) and the value obtained for A increases to $1160 \text{ cm}^{-1}\text{Å}$, in accordance with the mentioned hardening. Interestingly, this behavior is the opposite to what was observed for the carbon tubes³⁷, where there is a softening of the breathing mode for increasing curvature. Therefore, this effect must be related to an unique characteristic of the BN tubes as compare to the carbon nanotubes: the buckled structure of its surface. For small and moderate radius BN nanotubes, the B atoms lie somewhat closer to the nanotube axis than the N atoms. This buckling is of the order of 0.1 Å for the smallest nanotubes, but decreases rapidly with increasing radius²⁷. Fig. 6(b) shows how the nanotube atoms are displaced in the breathing mode. The values plotted are the magnitude of the radial displacement of B atoms (δR_B) divided by that of the N atoms (δR_N). For $\delta R_B/\delta R_N = 1$ the displacements are of equal magnitude, and we would have a pure breathing mode, just as in a carbon nanotube. The observed behavior is slightly different: for tubes with $r < 4$ Å the displacement of the N (outer) atoms is larger than that of the B (inner) atoms. This can be explained in a simple model as a consequence of the tendency to preserve in the pattern of displacements of this vibrational mode the bond angles of the buckled surface.

As is well known^{24,48,56}, the constant A can be estimated from the elastic constants of the plane,

$$A \approx \frac{1}{2\pi} \sqrt{\frac{C_{xxxx}}{\rho}} = \frac{1}{2\pi} v_{LA}^{2D}. \quad (8)$$

Using this equation we obtain the value $A=1135 \text{ cm}^{-1}\text{Å}$, which is in reasonable agreement with the value found by the direct calculation.

Finally, let us discuss the ability of the zone-folding approach to predict the frequencies of the active modes of BN nanotubes. In the figures 7 and 8 we plot the frequencies obtained from zone-folding side-by-side with those obtained directly from the nanotubes, in both cases including the electrostatic interactions. For clarity, this is done separately for intermediate frequencies (around 700 cm^{-1}) and for high frequencies (above 1250 cm^{-1}), and separately for $(n,0)$ and (n,n) nanotubes. Overall, we can say that zone-folding is capable of rather accurate estimations of the actual frequencies, particularly for nanotubes with radii larger than 4 Å. In this case even

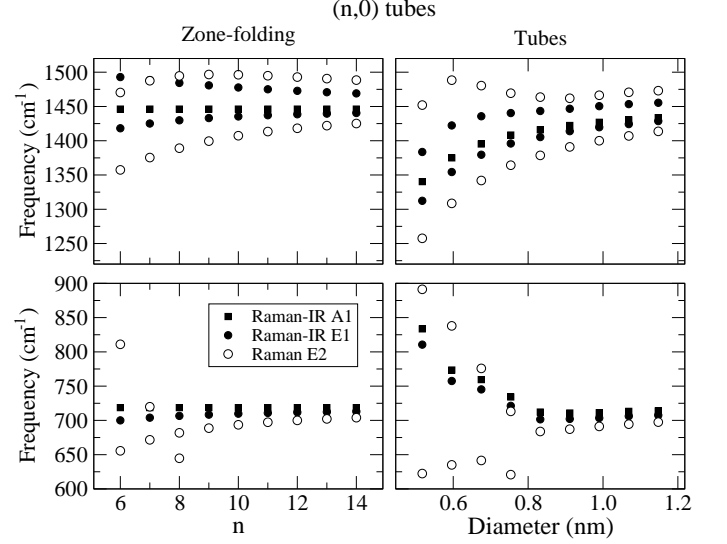


FIG. 7: Comparison between the optically active modes predicted by the zone-folding approximation and those obtained directly from the tubes geometry. Here we show the results for $(n,0)$ BN tubes with n running from 6 to 14. The modes have been classified according to their symmetry (the meaning of the symbols is the same in the four panels). For clarity, intermediate frequencies (around 700 cm^{-1}) and high frequencies (above 1250 cm^{-1}) are shown separately. See Ref. 52 for the numerical values of the frequencies.

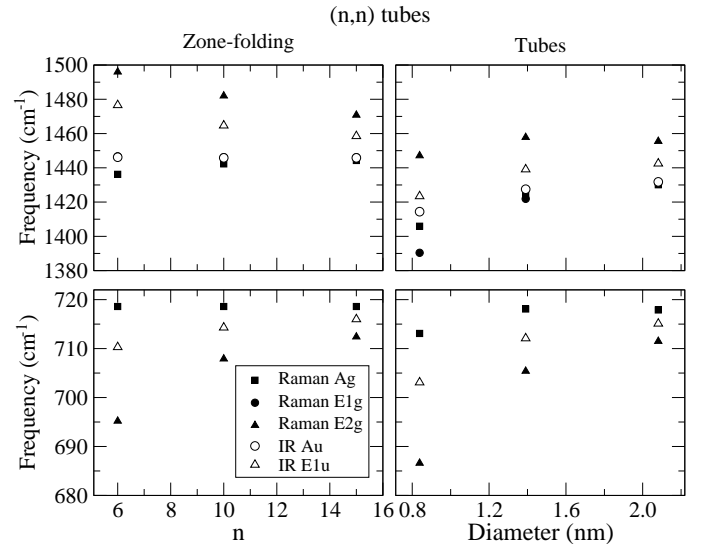


FIG. 8: Same as Fig. 7 but for (n,n) tubes, with $n=6,10$ and 15 . See Ref. 52 for the numerical values of the frequencies.

the ordering of the modes is accurately reproduced, both for $(n,0)$ and (n,n) tubes. The intermediate frequency modes are very well reproduced, but there is a slight over-estimation of the high-frequency modes, of the order of a few tens of wavenumbers.

That the zone-folding approach is capable of providing accurate estimates of the BN nanotube phonon frequencies rests on the absence of a $\mathbf{k} = 0$ (macroscopic) dipolar field in the BN monolayer. The reduced dimensionality of the system prevents the build up of a $\mathbf{k} = 0$ component of the electrostatic field, which thus only has a finite range. Therefore, no splitting of modes is observed at Γ ; the only effect of the electrostatic interactions is to shift slightly the high frequency modes and to confer a finite slope to the LO mode in the $\mathbf{k} \rightarrow \Gamma$ limit, modifications which do not prevent zone-folding from providing accurate estimates of the phonon modes of isolated nanotubes. A subtle point here is that the applicability of zone-folding in the case of BN also depends on the degree of transferability of the dielectric constant ϵ and the Born effective charges [see Eq.(2)] between the monolayer and nanotube geometries. For small nanotube radii there may be noticeable changes in the dielectric constant, but this is unlikely to affect the application of zone-folding to all but the narrowest nanotubes.

IV. SUMMARY AND CONCLUSIONS

In this work we have presented a detailed analysis of the vibrational properties of a BN monolayer, and of single-walled BN nanotubes of different diameters, including $(n,0)$, (n,n) and two chiral nanotubes. Our calculations are based on a non-orthogonal TB model complemented with long-range electrostatic interactions, not included in the TB model. The incorporation of these electrostatic interactions corrects to some extent the deficiencies of the TB model at intermediate and high frequencies in the BN layer. Using a simple model for a metal surface, we have analyzed the influence of placing a BN monolayer over such a surface on the phonon bands of the monolayer. The effect appears to be small and confined only to the high frequency range, above 1250 cm^{-1} . Generally, our calculated phonon frequencies, sound velocities and elastic constants are in good agreement with previous experimental and theoretical results. Concerning the nanotubes, we have obtained phonon band structures and have analyzed the optically active modes (IR and Raman) as a function of the nanotube structure and radius. We have also performed a detailed comparison between the predictions of the zone-folding approach and the actual frequencies of optically active modes obtained directly from the nanotubes, finding rather good agreement between the two for all except the narrower tubes, having radii below 4 \AA . High frequency mode frequencies are systematically overestimated by about a few tens of wavenumbers, but intermediate mode frequencies are given with high accuracy. Therefore, zone-folding should

also be useful in the context of BN nanotubes, as it has been in spectroscopic studies of carbon nanotubes. We also report on the behavior of the frequency and the pattern of atomic displacements of the radial breathing mode as a function of the tube radius.

Acknowledgments

The authors want to thank Prof. Pablo Ordejón for stimulating discussions. This work was supported in part by the Spanish Ministerio de Ciencia y Tecnología (grants MAT2001-0946, BFM2000-1312-C02 and BFM2002-03278), and by the Basque Departamento de Educación, Universidades e Investigación and the University of the Basque Country UPV/EHU (grant 9/UPV 00206.215-13639/2001). D.S.P acknowledges support from the Spanish Ministerio de Ciencia y Tecnología and CSIC under the "Ramón y Cajal" program.

APPENDIX: ABSENCE OF LO-TO SPLITTING FOR A BN MONOLAYER

In this appendix we briefly discuss the role of long-range electrostatic interactions in a monolayer, comparing the results with those found for bulk systems. Let us consider a thin slab of polar material parallel to the xy plane. We focus first in the in-plane optical modes, for which the atomic displacements \mathbf{u} are parallel to the xy plane. Associated with this phonon there is an electric polarization field $\mathbf{P} = \frac{1}{A}(\mathbf{Z}\mathbf{u})f(z)\cos(\mathbf{k}\cdot\mathbf{r})$ and a charge density $\rho_P = -\nabla\cdot\mathbf{P}$, where Z is the Born effective charge tensor within the unit cell, A is the area of the unit cell, and $f(z)$ is a function related to the profile (number of layers) of the slab which can be approximated by $\delta(z)$ for a monolayer. We stress that \mathbf{k} , \mathbf{u} , and \mathbf{P} are all parallel to the slab for pure in-plane modes. For the particular case of a system with hexagonal symmetry, like our BN sheets, the in-plane properties are isotropic, and Z can be regarded as a scalar. Although this is not crucial for our arguments, we will make this simplification in the following. The charge density ρ_P is proportional to the product $\mathbf{k}\cdot\mathbf{u}$, and no macroscopic charge accumulations appear due to the TO modes. However, a macroscopic electric field \mathbf{E}_{mac} can appear associated with the LO modes. The correct limit when $\mathbf{k} \rightarrow 0$ is then calculated by solving Poisson's equation for ρ_P . The components of the electric field in the directions parallel to the slab are

$$E_{mac}^i = \frac{4\pi}{A\epsilon} \frac{Z(\mathbf{k}\cdot\mathbf{u})}{k} k^i B(z,k) \cos(\mathbf{k}\cdot\mathbf{r}), \quad (\text{A.1})$$

where k is the modulus of \mathbf{k} , and $B(z,k)$ is given by

$$B(z,k) = \int_{-\infty}^{\infty} d\alpha \frac{\bar{f}(\alpha k) e^{-i(\alpha k z)}}{1 + \alpha^2}, \quad (\text{A.2})$$

$\bar{f}(q)$ being the Fourier transform of $f(z)$. Once the electric field has been calculated, the corresponding mod-

ification of the force-constants matrix can be obtained taken into account that the force acting on an atom is given by $\mathbf{F} = Z \mathbf{E}_{mac}$ ³³. In the case of the monolayer we take $f(z) = \delta(z)$, then $B(z = 0, k) = 1/2$ and the correction of the force-constants matrix for the in-plane modes becomes

$$C_{ij} = \frac{2\pi Z^2}{A \epsilon} \frac{k^i k^j}{k}. \quad (\text{A.3})$$

This correction goes to zero when $\mathbf{k} \rightarrow 0$ irrespective of the polarization of the mode and, therefore, both LO and TO in-plane modes have the same frequency. This is in agreement with the results obtained for slabs of ionic materials using different models^{57,58}: pure in-plane optical modes have frequencies close to those of the TO phonons in the bulk. It can also be noticed the linear behavior of the LO mode as it approaches Γ . We move now to analyze the bulk limit. By taking $f(z) = 1/L$, being L the distance between atomic layers, we can study the limit for bulk phonons with $k_z = 0$ (k_z is the wavevector perpendicular to the atomic layers in the bulk). $B(z, k)$ becomes now $1/(Lk)$, and the term in the force-constants matrix takes the usual form for bulk systems³³

$$C_{ij} = \frac{4\pi Z^2}{AL \epsilon} \frac{k^i k^j}{k^2}, \quad (\text{A.4})$$

which has a different value for LO and TO modes. For the intermediate case of a slab with finite thickness we find bulk behavior for phonons with sufficiently large k , while the behavior of the monolayer is recovered when k goes to zero. The slope of the LO modes at Γ is proportional to the number of layers in the slab.

For modes with polarization vectors having components along the normal to the slab (out-of-plane components within the nomenclature used throughout this paper) things can be quite different. For these modes, \mathbf{P} has a component along z and, when $k = 0$, the charge distribution ρ_p associated to them can be rationalized as a number of infinite planes with charges of alternating signs along z . There are also surface charges given by $\mathbf{P} \cdot \hat{\mathbf{n}} = P_z$. All these charged planes give rise to electric fields which do not decay along the entire thickness of the slab. In fact, those modes with atomic displacements perpendicular to the slab, although are *transversal* by definition (since the only phonon wavevector that can be safely defined is parallel to the slab), are known to have frequencies similar to those of the corresponding longitudinal phonons in the bulk^{57,58}. For this reason, Fuchs and Kliever⁵⁷ and Lucas⁵⁸ arrived to the conclusion that the phonon-frequency distribution of an ionic crystal slab converges very rapidly to that of bulk. However, for anisotropic systems like h-BN, where the frequency range of the in-plane and out-of-plane vibrations is very different, the conclusion might be different.

In the case of a free monolayer the separation between in-plane and out-of-plane modes is exact for an arbitrary wavevector \mathbf{k} . There is only one out-of-plane optical mode (ZO) which, although its frequency is slightly modified by the long-range interactions, cannot exhibit any splitting since it is a non-degenerate mode. The LO and TO in-plane modes do not exhibit splitting as explained above.

-
- * Email address: sqbsapod@sc.ehu.es
 § Email address: ehe@icmab.es
- ¹ H.W. Kroto, J.R. Heath, S.C. O'Brien, R.F. Curl, R.E. Smalley, *Nature* (London) **318** 162 (1985).
 - ² S. Iijima, *Nature* (London) **56** 354 (1991).
 - ³ M.M.J. Treacy, T.W. Ebbesen and M.J. Gibson, *Nature* (London) **381** 678 (1996).
 - ⁴ E.W. Wong, P.E. Sheehan and C.M. Lieber, *Science* **277** 1971 (1997).
 - ⁵ A. Krishnan, E. Dujardin, T.W. Ebbesen, P.N. Yianilos and M. M. J Treacy, *Phys. Rev. B* **58** 14013 (1998).
 - ⁶ J.-P. Salvetat, G. A. Briggs, J.-M. Bonard, R. R. Bacsa, A. J. Kulik, T. Stöckli, N. A. Burnham and L. Forró, *Phys. Rev. Lett.* **82**, 944 (1999).
 - ⁷ W.A. de Heer, A. Châtelain and D. Ugarte, *Science* **270** 1179 (1995); A.G. Rinzler, J. H. Hafner, P. Nikolaev, L. Lou, S. G. Kim, D. Tománek, P. Nordlander, D. T. Colbert and R. E. Smalley, *Science* **269** 1550 (1995).
 - ⁸ H. Dai, J. H. Hafner, A. G. Rinzler, D. T. Colbert and R. E. Smalley, *Nature* **384** 147 (1996).
 - ⁹ C. Dekker, *Physics Today*, 22 (May issue, 1999).
 - ¹⁰ P. G. Collins, K. Bradley, M. Ishigami and A. Zettl, *Science* **287**, 1801 (2000); J. Kong, N. R. Franklin, C. Zhou, M. G. Chapline, S. Peng, K. Cho and H. Dai, *Science* **287**, 622 (2000).
 - ¹¹ R. H. Baughman, A. A. Zakhidov and W. A. de Heer, *Science* **297**, 787 (2002); M. J. Biercuk, M. C. Laguno, M. Radosavljevic, J. K. Hyun, A. T. Johnson and J. E. Fishcher, *Appl. Phys. Lett.* **80**, 2767 (2002); D. Quian, E. C. Dickey, R. Andrews and T. Rantell, *Appl. Phys. Lett.* **76**, 2868 (2000).
 - ¹² P.M. Ajayan and T.W. Ebbesen, *Rep. Prog. Phys.* **60**, 1025 (1997); P.M. Ajayan, *Chem. Rev.* **99**, 1787 (1999); M. Terrones, W.K. Hsu, H.W. Kroto and D.R.M. Walton, *Topics in Current Chemistry* **199**, 189 (1999).
 - ¹³ M.S. Dresselhaus, G. Dresselhaus and P.C. Eklund, *Science of Fullerenes and Carbon Nanotubes* (Academic Press, New York 1996); T.W. Ebbesen (Ed.), *Carbon Nanotubes, Preparation and Properties* (CRC Press, Boca Raton 1997); P. J. Harris, *Carbon Nanotubes and Related Structures (New Materials for the Twenty-First Century)* (Cambridge University Press, Cambridge 2001).
 - ¹⁴ M. S. Dresselhaus and P. C. Eklund, *Adv. Phys.* **49**, 705-814 (2000).
 - ¹⁵ A. Jorio, A. G. Souza-Filho, G. Dresselhaus, M. S. Dresselhaus, A. K. Swan, M. S. Ünlü, B. B. Goldberg, M. A. Pi-

- menta, J. H. Hafner, C. M. Lieber and R. Saito, Phys. Rev. B **65**, 155412 (2002).
- ¹⁶ A. Jorio, R. Saito, J. H. Hafner, C. M. Lieber, M. Hunter, T. McClure, G. Dresselhaus and M. S. Dresselhaus, Phys. Rev. Lett. **86**, 1118 (2001).
- ¹⁷ A. Rubio, J.L. Corkill and M.L. Cohen, Phys. Rev. B **49** 5081 (1994)
- ¹⁸ X. Blase, A. Rubio, S.G. Louie and M.L. Cohen, Europhys. Lett. **28** 335 (1994).
- ¹⁹ N.G. Chopra, R.J. Luyken, K. Cherrey, V.H. Crespi, M.L. Cohen, S.G. Louie and A.Zettl, Science **269**, 966 (1995); A. Loiseau, F. Willaime, N. Demoncy, G. Hug and H. Pascard, Phys. Rev. Lett. **76**, 4737 (1996); M. Terrones, W.K. Hsu, H. Terrones, J.P. Zhang, S. Ramos, J.P. Hare, R. Castillo, K. Prasides, A.K. Cheetham, H.W. Kroto and D.R.M. Walton, Chem. Phys. Lett. **259**, 568 (1996); M. Terrones, A.M. Benito, C. Manteca-Diego, W.K. Hsu, O.I. Osman, J.P. Hare, D.G. Reid, H. Terrones, A.K. Cheetham, K. Prasides, H.W. Kroto and D.R.M. Walton, Chem. Phys. Lett. **257**, 576 (1996); K. Suenaga, C. Colliex, N. Demoncy, A. Loiseau, H. Pascard and F. Willaime, Science **278**, 653 (1997).
- ²⁰ L. Rapoport, Y. Bilik, Y. Feldman, M. Homyonfer, S.R. Cohen and R. Tenne, Nature (London) **387**, 791 (1997); Y. Feldman, E. Wasserman, D.J. Srolovitz and R. Tenne, Science **267**, 222 (1995); R. Tenne, L. Margulis, M. Genut and G. Hodes, Nature (London) **360**, 444 (1992).
- ²¹ Y. Li, J. Wang, Z. Deng, Y. Wu, X. Sun, D. Yu and P. Yang, J. Am. Chem. Soc. **123**, 9904 (2001).
- ²² R. S. Lee, J. Gavillet, M. Lamy de la Chapelle, A. Loiseau, J.-L. Cochon, D. Pigache, J. Thibault and F. Willaime, Phys. Rev. B **64**, 121405 (2001).
- ²³ Y. Miyamoto, M. L. Cohen and S. G. Louie, Phys. Rev. B **52**, 14971 (1995).
- ²⁴ K. N. Kudin, G. E. Scuseria and B. I. Yakobson, Phys. Rev. B **64**, 235406 (2001).
- ²⁵ G. Kern, G. Kresse and J. Hafner, Phys. Rev. B **59**, 8551 (1999).
- ²⁶ N. Ohba, K. Miwa, N. Nagasako, and A. Fukumoto, Phys. Rev. B **63**, 115207 (2001).
- ²⁷ E. Hernández, C. Goze, P. Bernier and A. Rubio, Phys. Rev. Lett. **80**, 4502 (1998).
- ²⁸ For a review on tight-binding see C.M. Goringe, D.R. Bowler and E. Hernández, Rep. Prog. Phys. **60** 1447 (1997).
- ²⁹ J. Widany, T. Frauenheim, T. Köhler, M. Sternberg, D. Porezag, G. Jungnickel and G. Seifert, Phys. Rev. B **53**, 4443 (1996).
- ³⁰ D. Porezag, T. Frauenheim, T. Köhler, G. Seifert and R. Kaschner, Phys. Rev. B **51**, 12947 (1995).
- ³¹ M. Elstner, D. Porezag, G. Jungnickel, J. Elsner, M. Haugk, T. Frauenheim, S. Suhai and G. Seifert, Phys. Rev. B **58**, 7260 (1998).
- ³² P. Ordejón, D. A. Drabold, R. M. Martin, and S. Itoh, Phys. Rev. Lett. **75**, 1324 (1995); W. Frank, C. Elsässer, and M. Fähnle, Phys. Rev. Lett. **74**, 1791 (1995).
- ³³ X. Gonze, J.-C. Charlier, D. C. Allan, and M. P. Teter, Phys. Rev. B **50**, R13035 (1994); X. Gonze and C. Lee, Phys. Rev. B **55**, 10355 (1997).
- ³⁴ For the construction of the Born effective charge tensor in the case of the tube geometry we have identified purely radial and tangential displacements with, respectively, out-of-plane and in-plane movements in the planar sheet. Therefore, for an atom i , which belongs to a tube of radius r and axis $(0,0,z)$, and occupies the position $(r \cos(\theta), r \sin(\theta), z_i)$, the Born effective charge tensor takes the form:
- $$Z_{\mu\nu}^i = \begin{pmatrix} (Z_{\perp}^i \cos^2(\theta) + Z_{\parallel}^i \sin^2(\theta)) & (Z_{\perp}^i - Z_{\parallel}^i) \cos(\theta) \sin(\theta) & 0 \\ (Z_{\perp}^i - Z_{\parallel}^i) \cos(\theta) \sin(\theta) & (Z_{\perp}^i \sin^2(\theta) + Z_{\parallel}^i \cos^2(\theta)) & 0 \\ 0 & 0 & Z_{\parallel}^i \end{pmatrix}$$
- ³⁵ R. Geick, C. H. Perry, and G. Ruppercht, Phys. Rev. **146**, 543 (1966).
- ³⁶ A. Kasuya, Y. Sasaki, Y. Saito, K. Tohji, and Y. Nishina, Phys. Rev. Lett. **78**, 4434 (1997).
- ³⁷ D. Sánchez-Portal, E. Artacho, J. M. Soler, A. Rubio and P. Ordejón, Phys. Rev. B **59**, 12678 (1999).
- ³⁸ In Ref. 24 some evidence was presented that, while for the small and moderate radius the strain energy is clearly smaller in the case of BN compared to C nanotubes, the opposite could be true for larger tubes ($r > 30 \text{ \AA}$). However, this seems quite unlikely if, as pointed out here, a smaller flexural rigidity of BN can already be deduced from the behavior of the ZA phonon band of the flat sheet. Unfortunately, the parameter δ is quite sensitive to the fit procedure and to numerical uncertainties, and the values for C and BN are close enough so no definitive conclusion can be given here.
- ³⁹ N. W. Ashcroft and N. D. Mermin, *Solid State Physics* (Saunders, Philadelphia 1976).
- ⁴⁰ C. Kittel, *Introduction to Solid State Physics*, (John Wiley, New York 1986).
- ⁴¹ In fact, the in-plane stiffness C reported in Ref. 24 should be compared with our Young modulus Y (Table I). The elastic constant C_{xxxx} is, in the notation of that reference, given by $C/(1 - \nu^2)$ with a value of 0.284 TPa nm and ν being the Poisson ratio.
- ⁴² L. D. Landau and E. M. Lifshitz, *Theory of Elasticity (Course of Theoretical Physics, Vol. 7)*, Pergamon Press, Oxford 1986.
- ⁴³ T. Kuzuba, K. Era, T. Ishii, and T. Sato, Solid State Commun. **6**, 523 (1968).
- ⁴⁴ R. J. Nemanich, S. A. Solin, and R. M. Martin, Phys. Rev. B **23**, 6348 (1981).
- ⁴⁵ D. M. Hoffman, G. L. Doll and P. C. Eklund, Phys. Rev. B **30**, 6051 (1984).
- ⁴⁶ E. Rokuta, Y. Hasegawa, K. Suzuki, Y. Gamou, C. Oshima and A. Nagashima, Phys. Rev. Lett. **79**, 4609 (1997).
- ⁴⁷ R. Saito, T. Takeya, T. Kimura, G. Dresselhaus and M. S. Dresselhaus, Phys. Rev. B **57**, 4145 (1998).
- ⁴⁸ G. D. Mahan, Phys. Rev. B **65**, 235402 (2002).
- ⁴⁹ V. N. Popov, V. E. Van Doren and M. Balkanski, Phys. Rev. B **61**, 3078 (2000).
- ⁵⁰ J. Yu, R. K. Kalia and P. Vashista, J. Chem. Phys. **103**, 6697 (1995).
- ⁵¹ B. I. Yakobson, C. J. Brabec, and J. Bernholc, Phys. Rev. Lett. **76**, 2511 (1996).
- ⁵² See EPAPS Document No. XXX (this number is provided by the PRB editor) for the tables containing the numerical values of the vibrational frequencies at Γ , including the Raman and IR active modes, for all the tubes studied in this work. The frequencies have been classified according to their symmetries. This document may be retrieved via the EPAPS homepage (<http://www.aip.org/pubservs/epaps.html>) or from

ftp.aip.org in the directory /epaps/. See the EPAPS homepage for more information.

- ⁵³ Similarly to the case of the monolayer, the main changes on the phonon band structure of the single-walled tubes induced by the long-range dipolar interactions are relatively small and restricted to the high-frequency modes: the in-plane optical modes extend over a somewhat larger energy range, and some of the longitudinal modes (with atomic displacements parallel to the tube axis) exhibit a larger dispersion with \mathbf{k} . These changes are directly related to the

larger overbending of the LO band of the BN monolayer when the electrostatic interactions are included.

- ⁵⁴ O. E. Alon, Phys. Rev. B **64**, 153408 (2001).
⁵⁵ O. E. Alon, Phys. Rev. B **63**, 201403 (2001).
⁵⁶ J. Kürti, G. Kresse, and H. Kuzmany, Phys. Rev. B **58**, R8869 (1998).
⁵⁷ R. Fuchs and K. L. Kliewer, Phys. Rev. **140**, A2076 (1965).
⁵⁸ A. A. Lucas, J. Chem. Phys. **48**, 3156 (1968).